# Electron-energy-loss investigation of hole-plasmon excitation due to thermal indiffusion boron doping of Si(111) surfaces

P. J. Chen
*Department of Physics, University of Pittsburgh, Pittsburgh, Pennsylvania 15260*

J. E. Rowe
*AT&T Bell Laboratories, Murray Hill, New Jersey 07974*

J. T. Yates, Jr.
*Surface Science Center, Department of Chemistry, University of Pittsburgh, Pittsburgh, Pennsylvania 15260*
(Received 14 July 1994)

High-resolution electron-energy-loss-spectroscopy (HREELS) measurements have been performed on Si(111) surfaces heavily *p*-doped by the decomposition of adsorbed decaborane with subsequent diffusion more than $\sim 1000$ Å below the surface. After thermal decomposition of the decaborane to produce B atoms on the surface the low-energy-electron-diffraction pattern shows a $\sqrt{3}\times\sqrt{3}$ periodicity due to $\frac{1}{3}$ ML of boron in the second complete layer. The HREELS data have two strong features: (1) the B-Si dipole vibrational mode at 96 meV and a broad electronic surface-plasmon mode at $\sim 100$ meV loss energy due to the free carriers in the region below the B-reconstructed surface layer. We have investigated the energy dependence of the plasmon mode in order to determine the possibility of using HREELS to determine the depth profile of the free carriers due to B diffusion into the region $\sim 50$–$500$ Å below the surface. Unexpectedly, we find that kinematic factors play an important role in the energy range used, 1.5–28 eV, and thus limit the degree of quantitative information that can be obtained about the carrier depth profile from HREELS data in this low-energy range. An approximate depth profile is deduced from the well-established three-layer model (vacuum-surface-bulk layers) after correcting the plasmon peak position for the kinematic factors.

## I. INTRODUCTION

An important parameter for the understanding of the space-charge region near the surface of a semiconductor is the doping density and the doping concentration profile or dependence on depth from the surface. Although sputter-profile analysis such as secondary-ion mass spectrometery (SIMS) can give the atomic concentration profile, direct measurements of the carrier concentration profile usually require contacts and/or interface formation with metals or other semiconductors. It is well known that one can probe the carrier density through the low-energy free-carrier plasmon excitation using high-resolution electron-energy-loss spectroscopy (HREELS)[1–6] since the probing depth can extend to $\sim 3000$ Å depending upon the excitation energy and the energy of the incident electrons. In this paper we report experiments using HREELS to probe the carrier-hole plasmon excitation in the space-charge region $\sim 50$–$500$ Å below the surface of Si(111) doped *p* type with B. We have explored the possibility of measuring the doping profile that occurs after *in situ* boron doping of the Si(111) surface by thermal diffusion of surface boron atoms produced by thermal decomposition of adsorbed decaborane molecules.

Although the basic idea of using HREELS to study free-carrier surface plasmons has been explored in a number of previous studies,[1–6] the B/Si(111) surface is unique in terms of the lack of intrinsic surface phonons present in II-VI or III-V compound semiconductors, and the lack of Fermi-level pinning.[7] The Fermi-level pinning for complete $\sqrt{3}\times\sqrt{3}$ occupation is near the top of the valence band as determined by photoemission spectroscopy.[7] Thus the depletion depth and space-charge band-bending potential are approximately zero and the analysis is somewhat simplified. This is an important advantage over other Si surfaces such as Si(100)$2\times1$ whose *n*-type doping was studied by Forster, Layet, and Lüth.[6] An effective carrier-hole concentration on the order of $\sim 10^{19}$ $cm^{-3}$ has been deduced from the HREELS measurements for monolayer-level boron initially deposited on the surface. The surface hole plasmon is highly damped due to the low mobility of carrier holes at such high concentrations and to the strong intravalence-band transitions resulting from the small spin-orbit splitting of the valence band for Si (35 meV). Under these conditions, kinematic effects in HREELS have to be taken into account in order to give a quantitative description of the electron-energy-loss features. Dipole scattering theory in conjunction with the long-wavelength Thomas-Fermi dielectric function gives an adequate description of the electron-energy-loss features. However, the ability of HREELS to probe different regions of the space-charge layer below the surface is limited by kinematic and finite spectrometer acceptance angle effects, especially at low incident electron energies. In spite of these difficulties we

 

deduce an approximate depth profile for this system using the well-known three-layer model (vacuum-surface-bulk layers) due to Mills and co-workers.[1,8]

## II. EXPERIMENTAL PROCEDURE

The HREELS measurements were performed in an ultrahigh-vacuum (UHV) system with a typical base pressure of $1\times10^{-10}$ mbar. The HREELS measurements ere carried out in the specular scattering geometry with a 60° incident angle at electron energies in the range 1.5–28 eV. The HREELS data were recorded in a pulse-counting mode at an energy increment of 0.6 meV, and are presented here without any post-acquisition data treatment. The boron deposition was carried out by thermally decomposing decaborane molecules[9,10] initially adsorbed on Si(111) at room temperature. Subsequent thermal annealing at 1200–1300 K promoted boron diffusion into the bulk of Si(111). In addition to an apparatus for HREELS, the chamber contained a cylindrical mirror analyzer for Auger-electron spectroscopy (AES) to characterize surface atomic composition and standard low-energy electron-diffraction (LEED) optics to observe surface order and periodicity. The details of this study are reported elsewhere.[10]

The surface structure of the B-modified $\sqrt{3}\times\sqrt{3}R30°$ Si(111) surface is shown in Fig. 1(a). The surface B atoms occupy the $S_5$ substitutional site, replacing surface Si atoms which now occupy the $T_4$ adatom sites to form an ordered $\sqrt{3}\times\sqrt{3}R30$ superstructure on top of the $(1\times1)$ bulk-terminated Si lattice. The B-atom subsurface $S_5$ site is in the first Si bilayer directly below the surface Si adatoms.[11–13] The nominal subsurface B concentration is 0.33 per $(1\times1)$ unit cell or $\frac{1}{3}$ monolayer.

The existence of an extensive body of knowledge of boron diffusion in Si allows a reliable estimation of the B diffusion length in Si(111) under our experimental conditions. For the B concentration of interest here, the diffusion is in the extrinsic regime, i.e., the diffusion coefficient is concentration dependent. Based on the annealing temperature and time, an empirical diffusion law based on the extrinsic model[14] gives an estimated diffusion length of $10^3$–$10^4$ Å. This distance has been verified by secondary-ion-mass spectroscopy (SIMS) measurements performed separately *ex situ* on the doped Si(111) crystals. Since the typical characteristic wave vector involved in dipole scattering is $\sim10^{-2}$ Å$^{-1}$ in HREELS,[1] the amplitude of excited plasma wave decays exponentially into the bulk on a scale ($\sim100$ Å) considerably less than the boron diffusion depth. Thus the B-doped region below the Si(111) surface is essentially doped uniformly with B-induced carriers in terms of its dynamic response to the low-energy electrons.

## III. EXPERIMENTAL RESULTS

### A. HREELS observation of the B-Si vibrational mode and surface hole-plasmon excitation

After boron deposition and annealing to form the ordered $(\sqrt{3}\times\sqrt{3})R30°$ surface, a typical HREEL spectrum taken at 100 K from the Si(111)-B$(\sqrt{3}\times\sqrt{3})R30°$ surface is shown in Fig. 1(b). There are two very distinct energy-loss features in the spectrum. The free-carrier surface-plasmon excitation in the highly B-doped region below the surface gives rise to a broad energy-loss feature centered at $\omega_{pp}=63$ meV. Superimposed on this background is a sharp loss peak at 96 meV (770 cm$^{-1}$) which is due to a B-Si vibrational mode (surface optical phonon) localized in the Si-B-Si surface triple layer. In an earlier work, Rowe *et al.* have characterized this mode as a breathing motion of B in the $S_5$ lattice site in Si. They found this mode at 102 meV in isotopically pure $B^{10}$ samples doped by ion implantation. In our work the dominant isotope is $B^{11}$, which accounts for the different excitation energy observed.

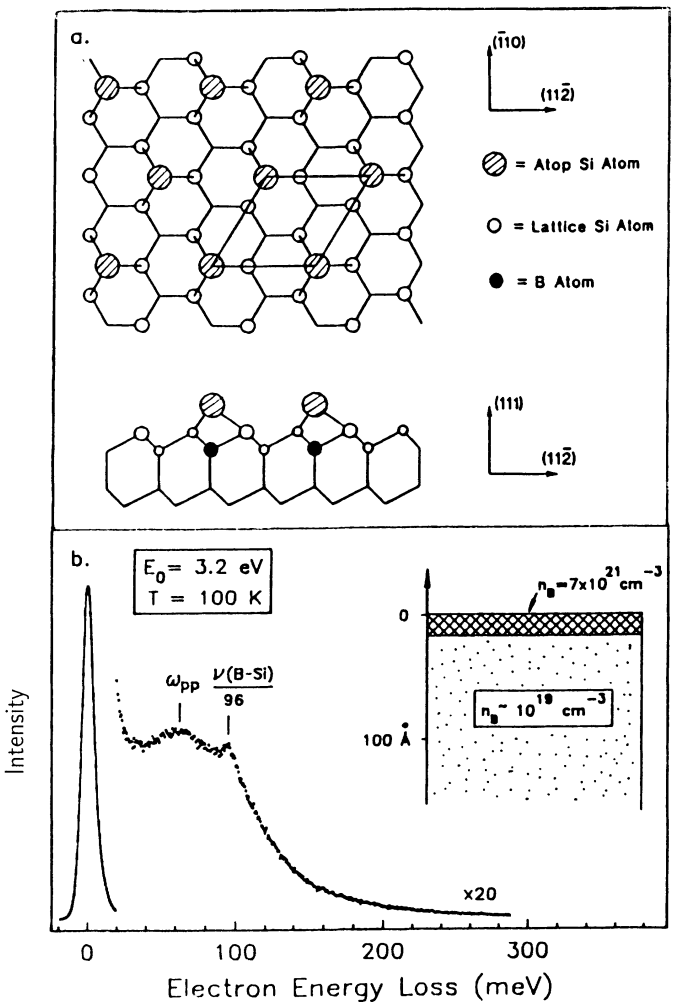


FIG. 1. (a) The structure of the Si(111)-B$(\sqrt{3}\times\sqrt{3})R30°$ surface with the $\sqrt{3}\times\sqrt{3}R30°$ unit cell outlined. The B atoms occupy the subsurface, substitutional $S_5$ sites in the first Si bilayer. (b) HREELS measurement of a well-ordered Si(111)-B$(\sqrt{3}\times\sqrt{3})R30°$ surface of 100 K with a primary electron energy $E_0=3.2$ eV. The peak position corresponding to the hole surface-plasmon low peak, $\hbar\omega_{pp}$, is at 63 meV. The loss peak belonging to the localized B-Si optical phonon mode is at 96 meV. The inset shows schematically the composition of the Si(111) crystal with the $\frac{1}{3}$-ML B layer displayed on an expanded scale.

Since the free-carrier plasmon energy is proportional to $n^{1/2}$ ($n$ is the carrier density), varying the doping level in Si is expected to have a direct effect on the observed peak position $\omega_{pp}$ due to the surface plasmon. This characteristic density dependence is verified qualitatively in the HREELS data (Fig. 2) taken at a constant electron energy $E_0=6.1$ eV on selectively B-doped Si(111) with increasing amounts of initial boron dose. For all but the highest exposure the surface plasmon peak position is proportional to the $\frac{1}{2}$ power of the surface B density measured by AES. This indicates that the rate of B diffusion into the bulk (and consequent density probed by HREELS) varies linearly with B surface concentration except at the highest exposures. It is also clear that the energy of the localized B-Si vibrational mode remains unaffected by the variation in $n$. Since this vibration is a local surface mode originating from the vibration of substitutional B atoms against the surrounding Si neighbors, the vibrational amplitudes are localized in the top two or three atomic layers. Unlike the more delocalized surface-optical phonons (the Fuchs-Kliewer modes) in bulk polar semiconductors such as GaAs,[3,4,16] this localized B-Si optical phonon is not expected to couple to the carrier surface plasmon and thus does not vary with plasmon energy.

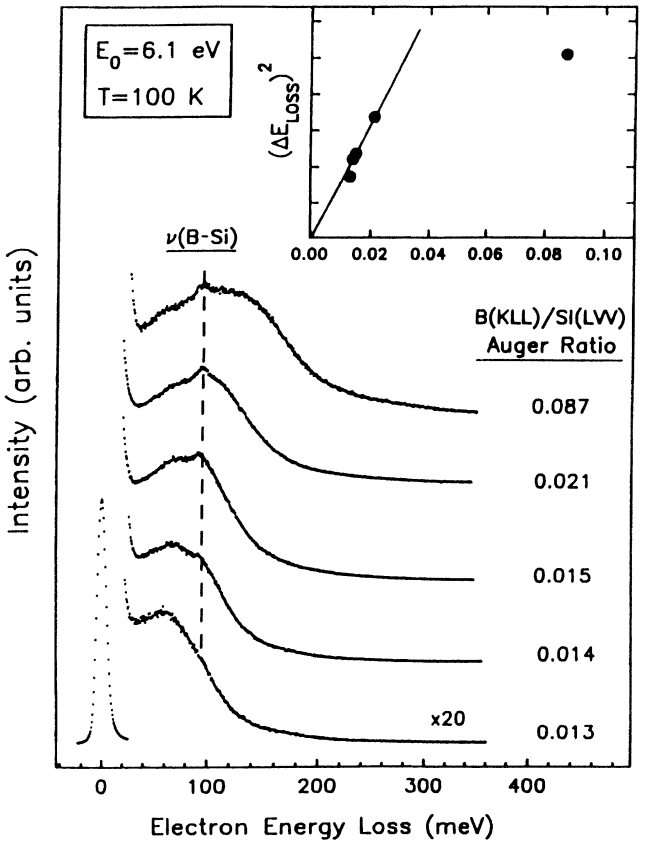


FIG. 2. HREELS measurements of surface hole-plasmon excitation on selectively B-doped Si(111). The incident electron energy is 6.1 eV at a 60° incident angle. The spectra correspond to increasing boron concentration in the near-surface region following successive boron deposition and annealing cycles. The inset shows a plot of $(\Delta E)^2$ vs the B/Si Auger ratio with $\Delta E=\hbar\omega_{pp}$.

### B. Electron energy dependence of hole-plasmon loss

Figure 3 shows a series of HREELS measurements taken at 100 K from a well-ordered $(\sqrt{3}\times\sqrt{3})R30°$ surface at various primary electron energies $E_0$. The intensity of the localized B-Si vibration decreases monotonically with increasing $E_0$. This behavior is consistent with the dipole scattering mechanism which has a $(1/E_0)^{1/2}$ dependence on the loss intensity.[1] Another prominent feature observed from these HREELS data curves is that the loss feature due to surface-plasmon excitation clearly shows a pronounced downshift in peak energy with decreasing $E_0$. Since the peak-position shift exhibited in the spectra *appears* to be similar to what was observed when boron concentration was changed, it might be tempting to interpret this phenomenon in the context of a changing carrier concentration $n$, as the effective probing depth of HREELS (to be defined below) varies with $E_0$. However, it has recently been demonstrated for GaAs (Refs. 17 and 18) that the kinematic factor in dipole scattering plays an important role in surface hole-plasmon excitation due to the high damping factor $\Gamma$ for low mobility $p$-type semi-

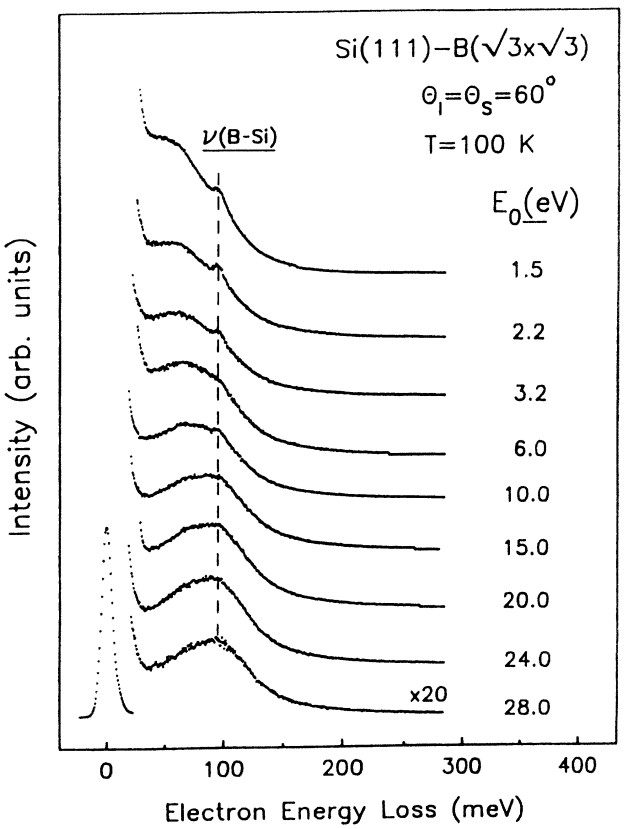


FIG. 3. HREELS measurement from a well-ordered Si(111)-B surface as a function of incident energy, $E_0$, at 100 K. The dashed line marks the energy of the B-Si vibrational mode, $h\nu$(B-Si).

conductors. Thus any quantitative interpretation of the $E_0$-dependent spectra obtained here has to take this factor into account. In order to fully address these physical issues contained in our experimental measurements, we next present a model dielectric function analysis of the electron-energy-loss cross section based on the well-known dipole scattering mechanism.[1] This is followed by a comparison of numerically simulated energy-loss spectra and experimental measurements. Finally we deduce an approximate free-carrier depth profile using the well-known three-layer model developed by Mills and coworkers[1,8] after correcting the measured plasmon peak position $\omega_{pp}$, for kinematic factors to yield the surface-plasmon energy $\omega_{sp}$.

## IV. THEORETICAL ANALYSIS

### A. Model dielectric function

We adopt a long-wavelength, local-dielectric-response theory upon which to base our model calculation and consider only a constant (uniform density) carrier concentration $n$ for simplicity. The dielectric response of the free-carrier holes is assumed to be described by the frequency- and wave-vector-dependent Thomas-Fermi dielectric function $\varepsilon_{TF}$:

$$\varepsilon_{TF}(\omega,\mathbf{k})=\varepsilon_\infty-\frac{4\pi e^2 n}{m[\omega^2+i\omega\Gamma-D(\mathbf{k})]}$$
$$=\varepsilon_\infty-\frac{\omega_p^2}{\omega^2+i\omega\Gamma-D(\mathbf{k})}\ , \tag{1}$$

with $D(\mathbf{k})=\frac{3}{5}\mathbf{k}^2 v_F^2$, where $v_F$ is the Fermi velocity, $\omega_p$ is the bulk plasma frequency, and $\varepsilon_\infty$ is the high-frequency dielectric constant. The damping factor $\Gamma$ is directly related to the carrier-hole mobility $\mu_h$ by

$$\Gamma=\frac{e}{m_h\mu_h}\ . \tag{2}$$

The effective mass of the carrier holes is taken from the contribution of both light and heavy holes in the form[17]

$$\frac{1}{m_h}=\frac{n_{lh}}{n_h m_{lh}}+\frac{n_{hh}}{n_h m_{hh}}\ , \tag{3}$$

where $n_{lh}$ and $n_{hh}$ are the concentration of light and heavy holes in Si.

In the limit of long wavelength and zero damping, the surface-plasmon frequency $\omega_{sp}$ is defined as

$$\omega_{sp}=\left[\frac{4\pi e^2 n}{m(\varepsilon_\infty+1)}\right]^{1/2}=\frac{\omega_p}{\sqrt{\varepsilon_\infty+1}}\ , \tag{4}$$

which relates $\omega_{sp}$ directly to $n^{1/2}$.

This choice of dielectric function is based on the following physical considerations for our system: (i) the $\mathbf{k}$ range involved in our near-specular HREELS measurements is at least one order of magnitude smaller than the Fermi wave vector $\mathbf{k}_F$ at the current carrier density ($\sim 5\times 10^{19}$ cm$^{-3}$) under study. Thus the experiments essentially explore the dielectric response of the system in the long-wavelength limit. (ii) At such a high doping level, the Thomas-Fermi screening length is very short (a few Å) compared to the depth ($\sim 10^3$ Å) of the free-carrier space-charge region. Thus a physical condition exists to apply the local dielectric response formalism. In addition, a quantitative comparison between the local response and a nonlocal theory[19,20] under accumulation layer conditions indicates reasonable agreement between the two at long wavelengths, the important region for dipole scattering geometry HREELS.

### B. Dipole scattering mechanism and kinematic effects

In the dipole scattering theory which describes the electron-energy-loss process due to collective excitations at a solid surface, the spectral intensity $I(\omega)$ or differential cross section (normalized to the elastic intensity) is represented in a two-dimensional (2D) momentum space integral[1,3] which contains a product term of the kinematic factor and the loss function $\mathrm{Im}[-1/(\varepsilon+1)]$ integrated over the parallel momentum-transfer range $Q_c$, defined by the spectrometer acceptance angle $\theta_c$:

$$I(\omega)=\frac{4e^2 v_\perp^2}{\pi^2\hbar^2}\left[\frac{\mathbf{k}_S}{\mathbf{k}_I}\right]\int_{Q<Q_c}\frac{\mathbf{Q}d^2\mathbf{Q}}{[v_\perp^2\mathbf{Q}1^2+(\omega-\mathbf{v}_\parallel\cdot\mathbf{Q})^2]^2}$$
$$\times[1+n(\omega)]\mathrm{Im}\left[\frac{-1}{\varepsilon(\omega,\mathbf{Q})+1}\right], \tag{5}$$

where $\mathbf{k}_I$ and $\mathbf{k}_S$ are the wave vectors of the incident and scattered electrons. Inside the $\mathbf{k}$-space integral, the kinematic factor acts as a weighing function on the loss function, $\mathrm{Im}[-1/(\varepsilon+1)]$, at each parallel momentum transfer $\mathbf{Q}$. If we are in the parameter regime of small damping, where the loss function consists of sharp peaks with narrow widths (such as the optical phonons in an ionic crystal), varying the kinematic factor only modulates the *intensities* of the energy-loss peaks in the final outcome of the $\mathbf{k}$-space integral in $I(\omega)$ (assuming small dispersion of $\varepsilon$). The loss peak positions essentially coincide with the poles in $\mathrm{Im}[-1/(\varepsilon+1)]$. On the other hand, if the low function contains a broad frequency response due to large damping, kinematic effects will then become important in determining the peak position in the differential cross section, $I(\omega)$. This latter case of loss function $\mathrm{Im}[-1/(\varepsilon+1)]$ is encountered in the current study of surface hole-plasmon excitation in the heavily B-doped Si(111) due to large damping. Again, under the conditions of negligible dispersion with $\mathbf{k}$, the energy position of the observed loss peak in $I(\omega)$ differs from the peak position of $\mathrm{Im}[-1/(\varepsilon+1)]$ by virtue of the strong $\omega$ dependence of the kinematic factor. At the highest doping levels currently achieved, the damping width of the hole plasmon, $\Gamma$, is comparable to the surface-plasmon frequency $\omega_{sp}$, due to strong scattering of carrier holes by the ionized dopant atoms. Under this circumstance, the observed loss peak position $\omega_{pp}$ can no longer be simply equated to $\omega_{sp}$ as defined by Eq. (4), and a full evaluation of $I(\omega)$ is generally necessary in order to

obtain $\omega_{sp}$, $n$, and $\Gamma$ from the measured energy-loss spectrum.

Another well-known aspect of the kinematic effect in dipole scattering is the selectivity in Q, the parallel momentum transfer, with varying $E_0$. At a given $E_0$ and for a given energy loss $\hbar\omega$, the kinematic factor (or the dipole angular lobe) peaks sharply at a particular wave vector $Q_0 \approx (\hbar\omega/2E_0)k_0$. Consequently, a region of the space-charge layer defined by an effective sampling depth, $d_{eff} \sim Q_0^{-1}$, is selectively probed by the low-energy electrons.[1] It has been suggested[1,3,4,20] that this property can be utilized as a potentially meaningful experimental tool to probe the dynamics of a nonuniform space-charge layer in a depth-resolved fashion, especially in the near-surface region ($10^2$–$10^3$ Å). However, by varying the incident electron energy $E_0$, not only the sampling depth $d_{eff}$ is changed, the kinematic factor is also effectively changed as well. Under the condition of large damping, the kinematic effects of varying $E_0$ should also be considered in interpreting the $E_0$-dependent plasmon loss spectra. This analysis for the B-doped Si(111) surface will be presented below with a numerical evaluation of Eq. (5) using parameters best representing our experimental conditions.

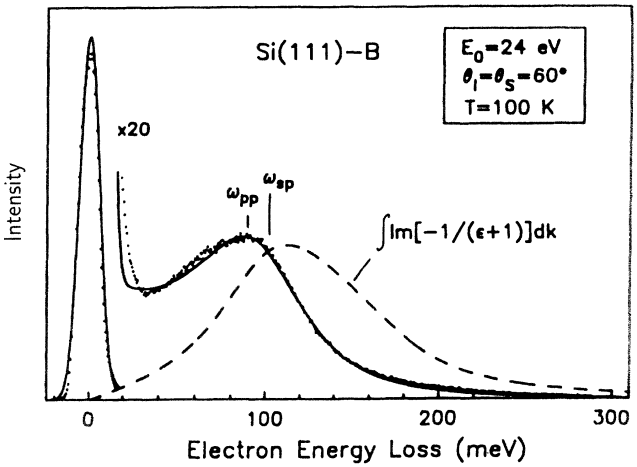


FIG. 4. Comparison between calculated and experimental HREELS loss intensity spectra. The solid theoretical curve is based on the Thomas-Fermi model dielectric function, $\varepsilon_{TF}$, and dipole scattering theory. The best fit to the experimental spectrum is obtained with $n_h = 5.4\times10^{19}$ cm$^{-3}$ and a damping factor $\Gamma = 74$ meV, which corresponds to a surface-plasmon frequency $\omega_{sp} = 102$ meV and a loss peak position $\omega_{pp} = 88$ meV. The dashed curve is the $k$-integrated lost function Im$[-1/(\varepsilon+1)]$. A Gaussian function with 11-meV FWHM has been used to simulate the elastic peak.

## V. COMPARISON BETWEEN THEORY AND EXPERIMENT

The model calculation incorporating both the dipole scattering kinematics and the model dielectric function is carried out numerically by assuming a circular spectrometer aperture and a fixed value of $\theta_c = 2.5°$. This will provide the basis for a more quantitative analysis of the experimental data and understanding of the physics contained in the HREELS measurements.

As a start, we apply the formalism outlined above to generate a theoretical energy-loss spectrum. The carrier density $n_h$ and damping factor $\Gamma$ are used essentially as fitting parameters to the experimental spectrum. Figure 4 shows the comparison between the measured data (points) and the fit (solid line). The overall quantitative agreement between theory and experiment is good. It should be pointed out that theoretical curve is not sensitive to $\theta_c$ because at $E_0 = 24$ eV, the scattered electron angular distribution is very narrow and the dipole lobe peaks only $\theta < 0.2°$ away from the specular direction. Virtually all the scattered electron intensity is collected by a spectrometer aperture, $\theta_c = 2.5°$, used in the calculation. The best fit yields $n_h = 5.4\times10^{19}$ cm$^{-3}$ and $\hbar\omega_{pp} = 88$ meV, which corresponds to $\hbar\omega_{sp} = 102$ meV. We treat the carrier density $n_h$ determined in this fashion as an "effective" carrier density which is an average over the distance of the effective electron sampling depth, $d_{eff}$, defined earlier. At $E_0 = 24$ eV, this distance is $d_{eff} \sim 220$ Å at the observed plasmon peak energy. The damping term $\Gamma$ is related to the carrier (hole) mobility $\mu_h$ through Eq. (3) given in Sec. IV A, from which a value $\mu_h = 54$ cm$^2$/V sec is obtained through the fitting. This value agrees well with the reported bulk hole mobility in heavily B-doped Si.[21] Also plotted in Fig. 4 (dashed curve) is the **k**-integrated loss function Im$[-1/(\varepsilon+1)]$, which is used to illustrate the effect of the kinematic factor. Its behavior shows that in the **k** range explored in HREELS, dispersion in $\varepsilon_{TF}$ has only a negligibly small effect on the energy-loss peak position. The dominating factor for shifting the peak position away from that of Im$[-1/(\varepsilon+1)]$ is the strong $\omega$ dependence of the kinematic factor. It is clear from Fig. 4 that when $\omega_{sp} \sim \Gamma$ the full spectrum $I(\omega)$ and the **k**-integrated loss function Im$[-1/(\varepsilon+1)]$ peak at different $\omega$ values. Note that *neither* peak position corresponds to the surface-plasmon energy $\omega_{sp}$, defined by Eq. (4). For precisely this reason, the determination of $n_h$ from the observed loss peak position is no longer straightforward. A simplified relation linking the observed loss peak position $\omega_{pp}$, and the surface-plasmon frequency $\omega_{sp}$ has been given by Meng *et al.*[17] under the approximation of a $1/\omega$-like behavior of the kinematic factor, i.e., the Drude model for the dielectric function.

Next we use the same fitting parameters to generate a set of simulated spectra with varying $E_0$. These results are shown in Fig. 5. Varying the electron energy $E_0$, as noted before, effectively varies the effective electron probing depth $d_{eff}$ *and* the kinematic factor. It can be seen from the calculated energy-loss spectra that the major effect is a modulation of the loss intensities. For electron energy $E_0 > 5$ eV, the loss peak position remains essentially unchanged. Below this electron energy, a widening dipole lobe which moves away from the specular direction results in an intensity cutoff on the high-energy-loss side due to a finite spectrometer acceptance aperture $\theta_c$. This high-energy-loss cutoff causes the overall weight of

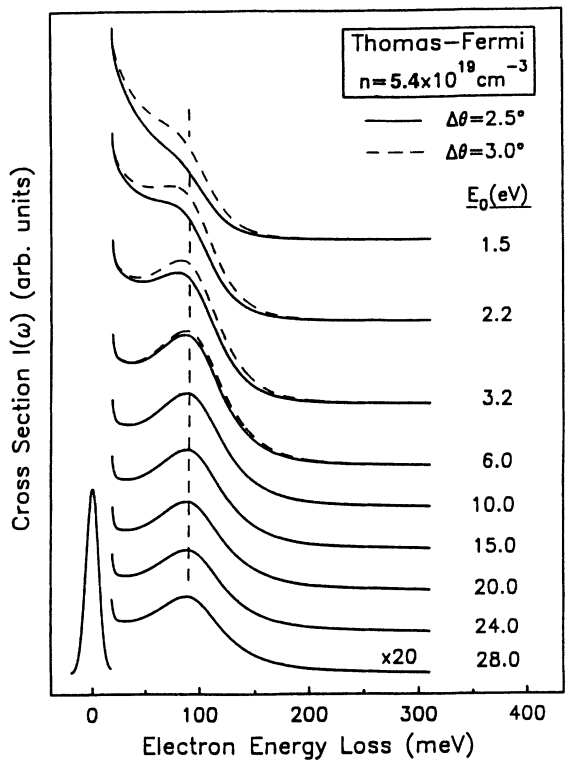


FIG. 5. Calculated energy-loss spectra $I(\omega)$ as a function of $\varepsilon_0$ based on the best-fit parameters discussed in the text. The solid curves are for a spectrometer acceptance angle $\theta_c = 2.5$, the dashed ones are for $\theta_c = 3.0$.

the energy-loss features to shift toward the lower-energy-loss side. Numerical calculation with two different $\theta_c$ values clearly indicates this effect, as shown in Fig. 5. Even with a constant carrier density $n_h$, such kinematic effects are strong under the condition of large damping of the loss function $\mathrm{Im}[-1/(\varepsilon+1)]$.

Comparison between the experimental data (Fig. 3) and the theoretical simulation in Fig. 5 shows reasonable qualitative agreement. The general behavior of the loss intensities exhibited in the experimental spectra are fairly well reproduced in the simulation. However, the experimental spectra show a more pronounced peak shift than the simple uniform density model dielectric function would predict at a physically reasonable spectrometer angular acceptance. This suggests that there is a contribution from a nonuniform carrier concentration profile (such as a depletion layer) in the near-surface region (0–200 Å) that enter into the measured energy-loss spectra. In order to extract quantitative information about the surface-plasmon energy as a function of incident energy $E_0$, we fit the spectra in Fig. 3 similarly to the method above. The damping parameter $\Gamma$, the plasmon energy $\omega_{sp}$, and a quadratic polynomial for stimulating the background due to the elastic peak are used as parameters. The damping parameter was found to be only weakly energy dependent, as was the quadratic background polynomial. In addition, a Voigt function at a fixed energy of 96 meV and width of 15 meV was used to represent the B-Si vibrational mode. The spectrometer aperture was chosen to be $\theta_c = 2.5°$. The results of this fitting procedure are shown in Fig. 6(a) for the peak position $\omega_{pp}$ and the surface-plasmon energy $\omega_{sp}$. Note that the surface-plasmon energy varys much more slowly with energy than the peak position, as expected from the detailed analysis at $E_0 = 24$ eV presented above.

The data in Fig. 6(a) were then modeled with the well-known three-layer model dielectric function derived by Mills and co-workers.[1,8] This model function uses the thickness of the surface dielectric region, $D_{eff}$, as an adjustable parameter. Initially we chose only the B-Si vibrational mode and an energy-independent constant dielectric function $\varepsilon_\infty = 11.7$, appropriate for an undoped full-depletion layer at the surface. However, this choice lead to an unexceptably steep decrease in the value of $\omega_{sp}$ at low energy for reasonable depletion depths, which contradicts the results shown in Fig. 6(a). Then we chose a surface dielectric function that had a finite doping level lower than that of the bulk, which was fixed at $5.4\times10^{19}$ $\mathrm{cm}^{-3}$. The resulting fit shown as the thin solid line of

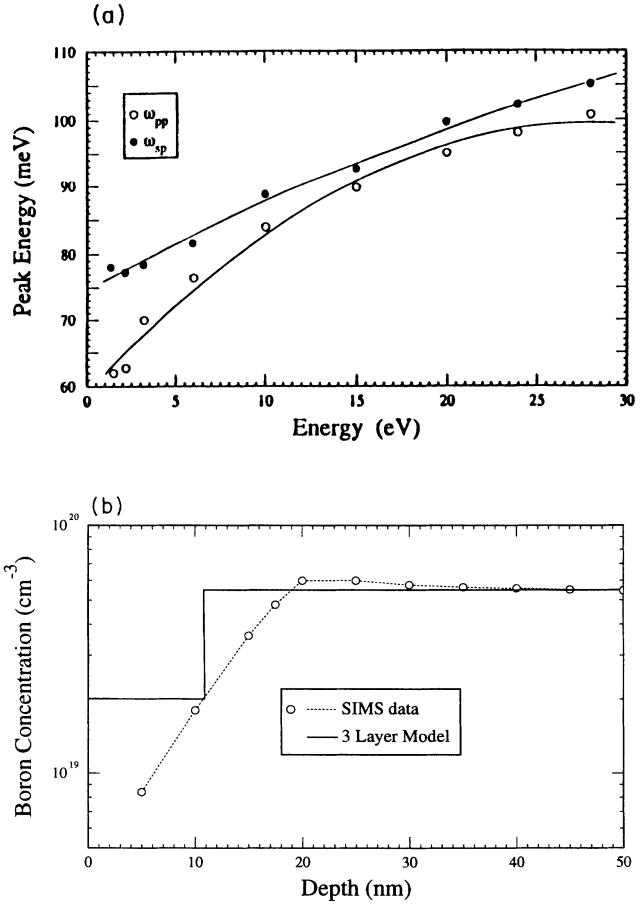


FIG. 6. Surface-plasmon energy $\omega_{sp}$ and observed plasmon peak position $\omega_{pp}$, plotted vs incident electron energy in part (a). The thin solid line for $\omega_{sp}$ is the result of a fit to the three-layer model (see text). The dashed line is a guide to the eye. Part (b) shows the depth dependence for the three-layer model and for measurements of the boron concentration using secondary ion mass spectrometery (SIMS).

Fig. 6(a) gave a surface layer thickness $D_{\text{eff}}=110$ Å, which compares with the average HREELS probing depth of 174 Å at $E_0=15$ eV. The surface doping level in the model was found to be $2\times10^{19}$ cm$^{-3}$. This density (over the surface layer thickness $D_{\text{eff}}=110$ Å) is a total number of carriers of $2.2\times10^{13}$ cm$^{-2}$, or 0.03 monolayers. The decreased carrier concentration may be due to the potential well for surface segregation of boron to maintain the surface monolayer at 0.33 monolayer for the reconstructed surface. Such a small number of carriers at this surface layer thickness produces only a weak $\sim kT$ amount of band bending which would be difficult to measure in photoemission.

The nonuniform carrier concentration over the HREELS probing depth (50–250 Å) is further substantiated by *ex situ* dynamical SIMS analysis performed on this Si(111) crystal, shown in Fig. 6(b) along with the result of the three-layer model fit. The sputter-profile measurement verifies the existence of boron concentration gradient which is characterized by a sharp decrease (about one order of magnitude) in boron concentration over the initial ~200 Å in depth. This trend is in good agreement with the result of the HREELS analysis presented above. The quantitative magnitude of the decreased B concentration measured by SIMS is likely to be influenced by the necessity of removing the sample from the UHV chamber. Exposing it to room air probably causes the very near-surface concentration to be influenced by oxidation prior to the SIMS measurement.

The dependence of the effective probing depth $d_{\text{eff}}$ on the electron energy has been discussed in the past. A number of studies (mostly on group III-V semiconductors) have been carried out[2–5,16–18] under various bulk doping conditions. Our current results clearly suggest that in the limit of small damping (such as for the high-mobility electron-doped III-V semiconductors), the utilization of the depth-probing capability of HREELS is more successful than other materials. However, when the plasmon damping $\Gamma$ becomes comparable to the plasmon energy $\hbar\omega_{\text{sp}}$, kinematic effects in HREELS due to finite momentum integration of the analyzer will limit the interpretation of the observed energy-loss spectra unless detailed corrections are made for the energy- and momentum-dependent kinematic factors.

Finally, we briefly discuss the role of the ordered $(\sqrt{3}\times\sqrt{3})R30°$ subsurface B layer which has been largely ignored in previous treatments. As a *p*-type dopant in bulk Si, B produces charge carriers (holes) in the Si valence band via thermal exitation of valence electrons into the B acceptor levels near the edge of the Si valence band. However, we argue that based upon the unique surface electronic structure of the boron-modified Si(111), the ordered $\frac{1}{3}$-ML B atoms are *electrically inactive* in terms of fulfilling their usual acceptor function. Because of the termination of the bulk crystal structure and the $(\sqrt{3}\times\sqrt{3})R30°$ surface reconstruction, these subsurface B atoms no longer provide similar acceptor levels near the edge of the Si valence band as bulk dopant B atoms do. The B-induced band-gap surface states lie 1.3–1.8 eV above the valence-band maximum (VBM),[22,23] and remain unoccupied at 100 K while the electron density originally associated with the surface Si adatoms redistributes toward the subsurface B, producing an occupied surface state below the VBM. As a result, no charge carriers (holes) are produced in the bulk Si valence band by these specially coordinated subsurface B atoms, and no band bending occurs. In the energy range of interest here, the dielectric response of this near-surface layer only comes from the B-Si optical phonon plus the contributions from the ion cores and possible two-dimensional plasmons which have been discussed for the B/Si(111) surface in previous work.[15,24]

## VI. SUMMARY AND CONCLUSIONS

We have used HREELS to explore the dielectric response in the near-surface region of a highly B-doped Si(111) crystal. The main conclusions can be summarized as follows.

(1) Following the thermal diffusion of boron in Si(111), surface-plasmon excitation due to the free-carrier holes has been observed by specular scattering HREELS at 100 K in the electron energy range 1.5–28 eV. The hole plasmon is highly damped due to the scattering of carriers by the ionized dopants and contributions from intravalence-band transitions.

(2) The dipole scattering theory combined with a Thomas-Fermi model dielectric function has been shown to provide a proper description of the electron-energy-loss cross section. Kinematic effects have to be taken into account in order to make a quantitative interpretation of experimental electron-energy-loss features and deduce the surface-plasmon frequency $\omega_{\text{sp}}$.

(3) At very low electron energies ($E_0<5$ eV), the combination of strong damping and finite spectrometer acceptance angle cutoff complicates the quantitative interpretation of the experimental HREELS data.

(4) Evidence for a nonuniform carrier concentration in the near-surface region ($\lesssim300$ Å) has been found by comparison of HREELS data and model calculations using the well-known three-layer model with a surface doping density about 0.4 that of the bulk. The lower density may be due to the strong tendency of B atoms to segregate to the reconstructed surface layer which competes with the bulk indiffusion.

## ACKNOWLEDGMENTS

We thank L. C. Feldman for carrying out nuclear activation analysis on our Si(111) crystals, and L. Hopkins for assistance with the SIMS measurements. The experimental help from M. L. Colaianni is also gratefully acknowledged. We acknowledge the financial support of this work by the Office of Naval Research.

[1]H. Ibach and D. L. Mills, *Electron Energy Loss Spectroscopy and Surface Vibrations* (Academic, New York, 1982), pp. 79–84.
[2]J. A. Stroscio and W. Ho, Phys. Rev. Lett. **54**, 1573 (1985).
[3]L. H. Dubois, B. R. Zegarski, and B. N. J. Persson, Phys. Rev. B **35**, 9128 (1987).
[4]Z. J. Gray-Graychowski, R. G. Egdell, B. A. Joyce, R. A. Stradling, and K. Woodbridge, Surf. Sci. **186**, 482 (1987).
[5]J. M. Seo, D. S. Black, P. H. Holloway, and J. E. Rowe, J. Vac. Sci. Technol. A **6**, 1523 (1988).
[6]A. Förster, J. M. Layet, and H. Lüth, Appl. Surf. Sci. **41/42**, 306 (1989).
[7]J. E. Rowe, G. K. Wertheim, and D. M. Riffe, J. Vac. Sci. Technol. A **9**, 1020 (1991).
[8]H. Froitzhiem, H. Ibach, and D. L. Mills, Phys. Rev. B **11**, 4980 (1975).
[9]Ph. Avouris, I.-W. Lyo, F. Boszo, and E. Kaxiras, J. Vac. Sci. Technol. A **38**, 3405 (1990).
[10]P. J. Chen, M. L. Colaianni, and J. T. Yates, Jr., J. Appl. Phys. **72**, 3155 (1992).
[11]R. L. Headrick, I. K. Robinson, E. Vlieg, and L. C. Feldman, Phys. Rev. Lett. **63**, 1253 (1989).
[12]P. Bedrossian, R. D. Mead, K. Mortensen, D. M. Chen, J. A. Golovchenko, and D. Vanderbilt, Phys. Rev. Lett. **63**, 1257 (1989).
[13]I.-W. Lyo, E. Kaxiaras, and Ph. Avouris, Phys. Rev. Lett. **63**, 1261 (1989).
[14]S. M. Sze, *Semiconductor Devices* (Wiley, New York, 1985), p. 391.
[15]J. E. Rowe, R. A. Malic, E. E. Chaban, R. L. Headrick, and L. C. Feldman, J. Electron Spectrosc. Relat. Phenom. **54/55**, 1115 (1990).
[16]Y. Chen, S. Nannarone, J. Schaefer, J. C. Hermanson, and G. J. Lapeyre, Phys. Rev. B **39**, 7653 (1989).
[17]Y. Meng, J. R. Anderson, J. C. Hermanson, and G. J. Lapeyre, Phys. Rev. B **44**, 4040 (1991).
[18]Y. Meng, J. Anderson, and G. J. Lepeyre, Phys. Rev. B **45**, 1500 (1992).
[19]B. Xu and J. C. Hermanson, Phys. Rev. B **40**, 12 539 (1989).
[20]D. H. Ehlers and D. L. Mills, Phys. Rev. B **36**, 1051 (1987).
[21]G. Masetti, M. Severi, and S. Solmi, IEEE Trans. Electron Dev. **30**, 764 (1983).
[22]Y. Ma, J. E. Rowe, E. E. Chaban, C. T. Chen, R. L. Headrick, G. M. Meigs, S. Modesti, and F. Sette, Phys. Rev. Lett. **65**, 2173 (1990).
[23]E. Kaxiras, K. C. Pandey, F. J. Himpsel, and R. Tromp, Phys. Rev. B **41**, 1262 (1990).
[24]M. Fontaine and J. M. Layet, J. Electron Spectosc. Relat. Phenom. **64/65**, 201 (1993).